minerals

MDPI

Article

The Provenance and Tectonic Settings of the Kolyma–Omolon Margin During the Closure of the South Anyui Ocean

Elena Vatrushkina [1,*], Elena Starikova [2], Alexander Khanchuk [1] and Aina Gagieva [3]

[1] Geological Institute, Russian Academy of Sciences, 7 bld.1, Pyzhevsky Lane, Moscow 119017, Russia; axanchuk@mail.ru
[2] Karpinsky All-Russia Research Geological Institute, 74 Sredny Prospekt, Saint Petersburg 199106, Russia; elena_starikova@karpinskyinstitute.ru
[3] Shilo North-East Interdisciplinary Scientific Research Institute, Far East Branch, Russian Academy of Sciences, 16, Portovaya St., Magadan 685000, Russia; gagieva@neisri.ru
* Correspondence: evat_095@mail.ru

Abstract

The Late Jurassic–Early Cretaceous Oloy complex was formed in the setting of convergence between the Chukotka microcontinent and the Kolyma–Omolon margin. Its evolution reflects the closure of the South Anyui Ocean, with controversial timing estimates. This study emphasizes the integration of lithological data with magmatic and metallogenic information to reconstruct geodynamic processes. The article presents the results of detailed petrographic and geochemical studies, Sm-Nd isotope analyses, and U-Pb dating of detrital zircons from Kimmeridgian–Lower Hauterivian volcaniclastic and epiclastic sandstones. Petrographic studies and U-Pb dating of detrital zircons identified the main sources at different stages and the amount of synchronous pyroclastic material. Isotope-geochemical investigations suggest a young undifferentiated arc provenance for Kimmeridgian deposits, whereas Tithonian–Valanginian sediments accumulated due to the erosion of more differentiated igneous rocks and input of clastic material from the continent. New data on changes in sedimentation environments and provenance enabled the tracing of the evolution of the Oloy arc. In the Kimmeridgian, the Oloy island arc existed on a heterogeneous basement, with south-dipping subduction towards the Kolyma–Omolon margin. During the Late Tithonian, the arc accreted and magmatic activity continued in the active margin setting. Collision initiated in the latter half of the Berriasian, reaching its active phase in the Valanginian time.

Keywords: Kolyma–Omolon margin; Upper Jurassic–Lower Cretaceous; volcaniclastic deposits; provenance; arc accretion; collision

Check for updates

Academic Editor: Georgia Pe-Piper

Received: 22 February 2026
Revised: 31 March 2026
Accepted: 12 April 2026
Published: 15 April 2026

Copyright: © 2026 by the authors. Licensee MDPI, Basel, Switzerland. This article is an open access article distributed under the terms and conditions of the Creative Commons Attribution (CC BY) license.

1. Introduction

The Late Jurassic–Early Cretaceous suprasubduction Oloy complex was formed during the convergence between the Chukotka block (as part of the Arctic Alaska–Chukotka microplate) and the Kolyma–Omolon continent [1–6]. According to most researchers [2,4,5,7–9], their collision was completed in the Barremian–Aptian (approximately 125–120 Ma), leading to the closure of the South Anyui Ocean which had previously separated them. However, some researchers [10] conclude that the South Anyui Ocean closed in the Late Jurassic. New data on the collisional nature of granitoids with an age of 144–135 Ma suggest its closure in the Late Berriasian–Valanginian [11]. During the Late Jurassic period, two subduction zones were reconstructed in the South Anyui

Ocean [1,2,5,6]. One of these existed in the northern part of the ocean near the Chukotka margin during the Oxfordian–Kimmeridgian time [5,6,12,13]. In the south, within the second zone, volcanic–plutonic and volcaniclastic rocks of the Oloy complex were formed. The southward direction of this subduction zone towards the Kolyma–Omolon continent is evidenced by the position of the suprasubduction volcanic complex relative to the accretionary prism [5]. Initially, based on the presence of marine volcaniclastic sequences and calc-alkaline volcanic rocks, the Oloy complex was regarded as an island-arc assemblage [1]. This suggestion was supported by the presence of low-Ti, high-Mg basalts and andesites of ensimatic origin in the frontal parts of the zone [14]. Later, based on the occurrence of Upper Jurassic–Lower Cretaceous rocks on the differently aged segments of the Kolyma–Omolon margin, combined with new data on the composition of both volcanic and plutonic rocks, the Oloy complex was reinterpreted as a volcanic–plutonic belt on the active margin of the Kolyma–Omolon continent [2,5,6]. The coexistence of rocks with intra-oceanic and continental affinities within this belt has been explained by its formation on a heterogeneous basement [4,14]. Additionally, it has been proposed that the units comprising the intra-oceanic arc were accreted to the Kolyma–Omolon continent during the Jurassic–Early Cretaceous, while the more evolved rocks of the Oloy arc were interpreted as parts of a continental-margin arc [7]. Recent geochemical studies of volcanic–plutonic rocks have shown that the Oloy complex formed in an island-arc setting and its subsequent accretion [15]. There is also no consensus regarding the age of the Oloy belt: some refer to the Tithonian–Berriasian (150–137 Ma) [7] or Kimmeridgian–Valanginian (154–135 Ma) [2], while others believe in an earlier origin (160 Ma) [16], in the Middle Jurassic (about 164 Ma) [3,6].

Interest in studying the Oloy suprasubduction complex has increased due to the fact that the main consumption of the oceanic lithosphere of the South Anyui basin occurred here up until the onset of collision [5], while the cessation of the Northern subduction zone occurred earlier. The emplacement of Cretaceous multiphase plutons is also associated with the formation of porphyry copper systems in the Baimka Trend, including the world-class Cu-Mo-Au Peschanka deposit [4,7,17].

The magmatic rocks of the Oloy complex have been studied in great detail. U-Pb dating of intrusions [6,7,17–19] and volcanic rocks [15,20] has been performed, and their geochemical characteristics have been studied [11,15,21]. However, the volcaniclastic sequences, which constitute a significant part of the section, remain unstudied by methods of sedimentary provenance analysis.

This article presents new data on the composition, geochemistry, Sm-Nd isotope system, and U-Pb age of detrital zircons from Kimmeridgian to Lower Hauterivian volcanic–sedimentary deposits of the Oloy complex of the Kolyma–Omolon margin. These data are used to interpret the tectonic settings of the sedimentary basin. The results obtained are intended to trace the evolution of the Oloy arc and determine how the geodynamic settings changed on the southern margin of the South Anyui Ocean during its closure stage.

2. Geological Background

2.1. Regional Geology

The studied region comprises the Chukotka, Omolon, Yarakvaam, Oloy, and South Anyui terranes. The collage is unconformably overlain by the Aptian–Albian post-collisional coal-bearing siliciclastic deposits and volcanic series. The uppermost position is occupied by the Late Albian and Late Cretaceous Okhotsk–Chukotka volcanic belt that has been interpreted as a major continental-margin arc (Figure 1).

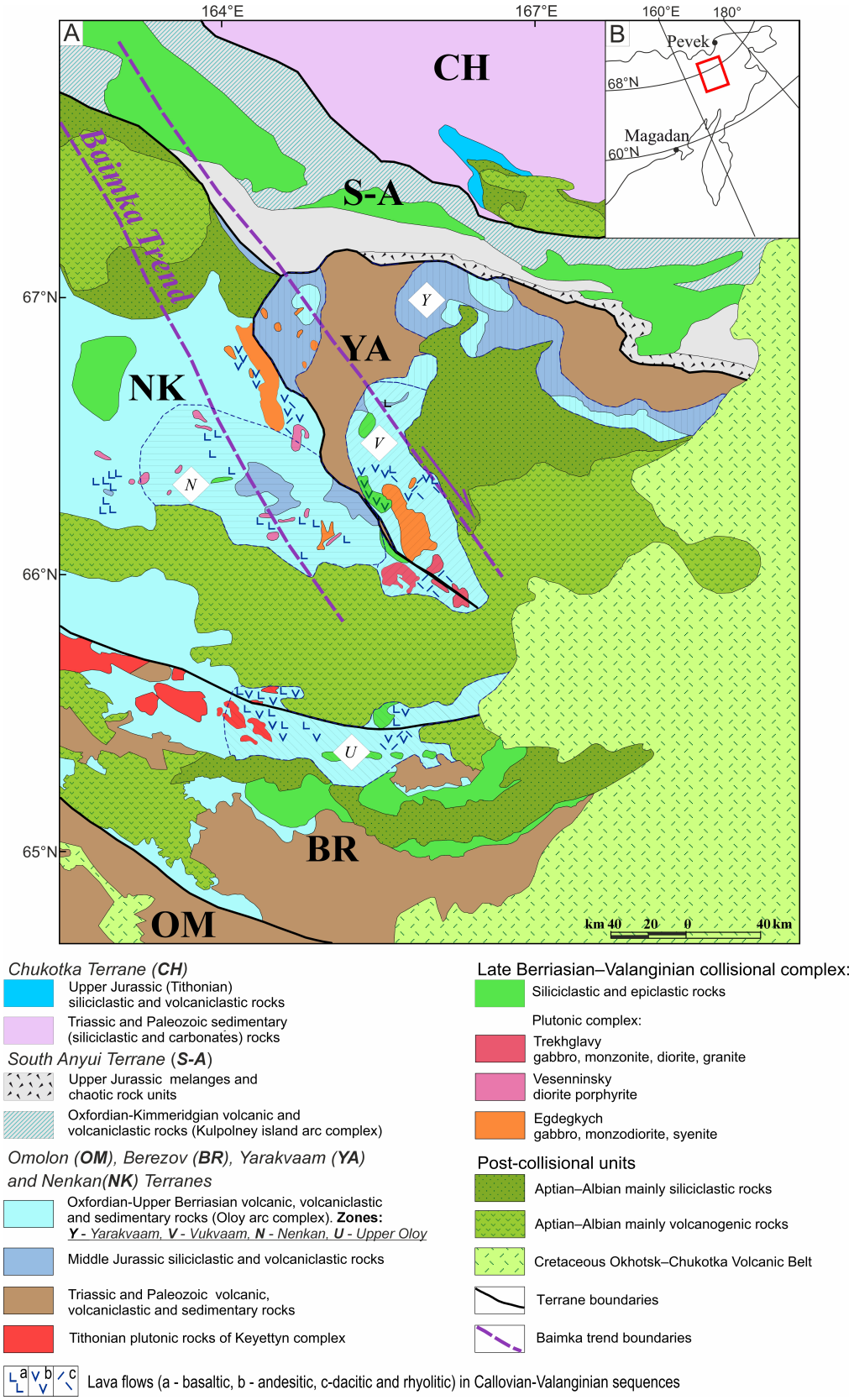


Figure 1. Tectonic scheme of Western Chukotka, modified following [11] (**A**) and location map (**B**).

The Chukotka terrane has a Neoproterozoic metamorphic basement and deformed Paleozoic–Mesozoic cover [2–4,22]. The accumulation of sedimentary deposits (siliciclastic and carbonates) in the Paleozoic occurred in a platform setting [23]. Large-thickness

Triassic turbidite sequences formed in passive continental margin conditions [24]. Upper Jurassic–Lower Cretaceous (Oxfordian–Valanginian) rocks are distributed in separate depressions. Oxfordian–Kimmeridgian and Valanginian deposits are mainly composed of arkosic sandstones with minor amounts of synchronous ash material. Tithonian–Berriasian deposits are mainly represented by volcaniclastic sequences. Interlayers of volcanic rocks are found only in one of the depressions to the east of the study area [12,25].

The Omolon cratonal terrane has an Archean to Paleoproterozoic crystalline basement metamorphosed to granulite and amphibolite facies, with U-Pb ages of 1.9 to 3.2 Ga [26]. The cover sequence consists of Neoproterozoic low-grade metasediments and Paleozoic platformal rocks, which accumulated intermittently [27,28]. Several rifting stages can be traced in the Omolon craton evolution (Neoproterozoic, Silurian, and Early–Middle Jurassic), which are associated with the emplacement of small intrusive bodies [28]. The most extensive manifestations of magmatism are recorded on Omolon in the Late Devonian Epoch, when suprasubduction volcanic–plutonic complexes were formed. Their geochemical characteristics suggest that they formed in an active continental margin setting [28,29].

The Berezov Paleozoic island-arc terrane is adjacent to the Omolon craton from the north. The basement is composed of deformed Middle–Upper Paleozoic (Devonian–Permian) andesite–rhyolite volcanites, volcaniclastic rocks, limestones, siliceous mudstones and siliciclastic rocks from mudstones to conglomerates (mainly in the upper part of the section). Paleozoic rocks are overlain by Late Jurassic–Early Cretaceous volcanic and volcaniclastic rocks of the Oloy complex.

The Yarakvaam Paleozoic island-arc terrane has a melanocratic Carboniferous–Permian basement composed of the Aluchin and Gromadnen–Vurguveem ophiolites in association with an island-arc volcanic complex [30]. Triassic and Lower–Middle Jurassic deposits, predominantly siliciclastic, overlie the Paleozoic strata [31–33]. The Upper Jurassic section varies from siliciclastic to volcaniclastic and volcanogenic, depending on the zone [31,32].

The Omolon cratonal terrane and Berezov and Yarakvaam Paleozoic island-arc terranes are part of KOM—the Kolyma–Omolon superterrane. According to most researchers, their amalgamation occurred in the Middle Jurassic [2–4,22].

The South Anyui terrane is a suture zone with a complex structure [4–6]. There is no consensus among researchers regarding the composition, age and origin of its constituent complexes [5,6,31]. Nevertheless, most researchers confidently distinguish a basalt–chert association of Bajocian–Kimmeridgian age [33] or, according to other estimates, Late Bathonian–Oxfordian age [31]. The Late Jurassic (Oxfordian–Kimmeridgian) volcanic–plutonic complex and volcaniclastic formations are of an oceanic island-arc origin [5,13,31]. The Lower Cretaceous (Berriasian–Valanginian) strata are predominantly composed of siliciclastic sequences with rare interbeds of volcaniclastic deposits [5,6,31]. According to Sokolov S. D. [22], the accretionary prism is composed of siliciclastic and volcaniclastic turbidites and a melange with blocks of oceanic crust (basalt, chert, gabbro, plagiogranite, and amphibolite). Tectonic sheets of the basalt–chert association are also found here. Siliciclastic rocks contain Tithonian and Berriasian–Valanginian fauna, while cherts contain Bajocian–Callovian and Oxfordian–Kimmeridgian radiolarians [22,31,33].

2.2. Lithology and Stratigraphy of Middle Jurassic–Lower Cretaceous (Aalenian–Hauterivian) Volcanic–Sedimentary Deposits of the Kolyma–Omolon Margin

Based on the section structure, the Middle Jurassic–Lower Cretaceous deposits in the northeastern part of the Kolyma–Omolon superterrane can be divided into four main zones (Figure 2). Accumulation occurred in a marine setting. The sequences are dated sufficiently precisely based on fauna [15,31–33]. This enabled the construction of com-

posite sections for each zone and their correlation, despite poor outcrop conditions and intensive deformations.

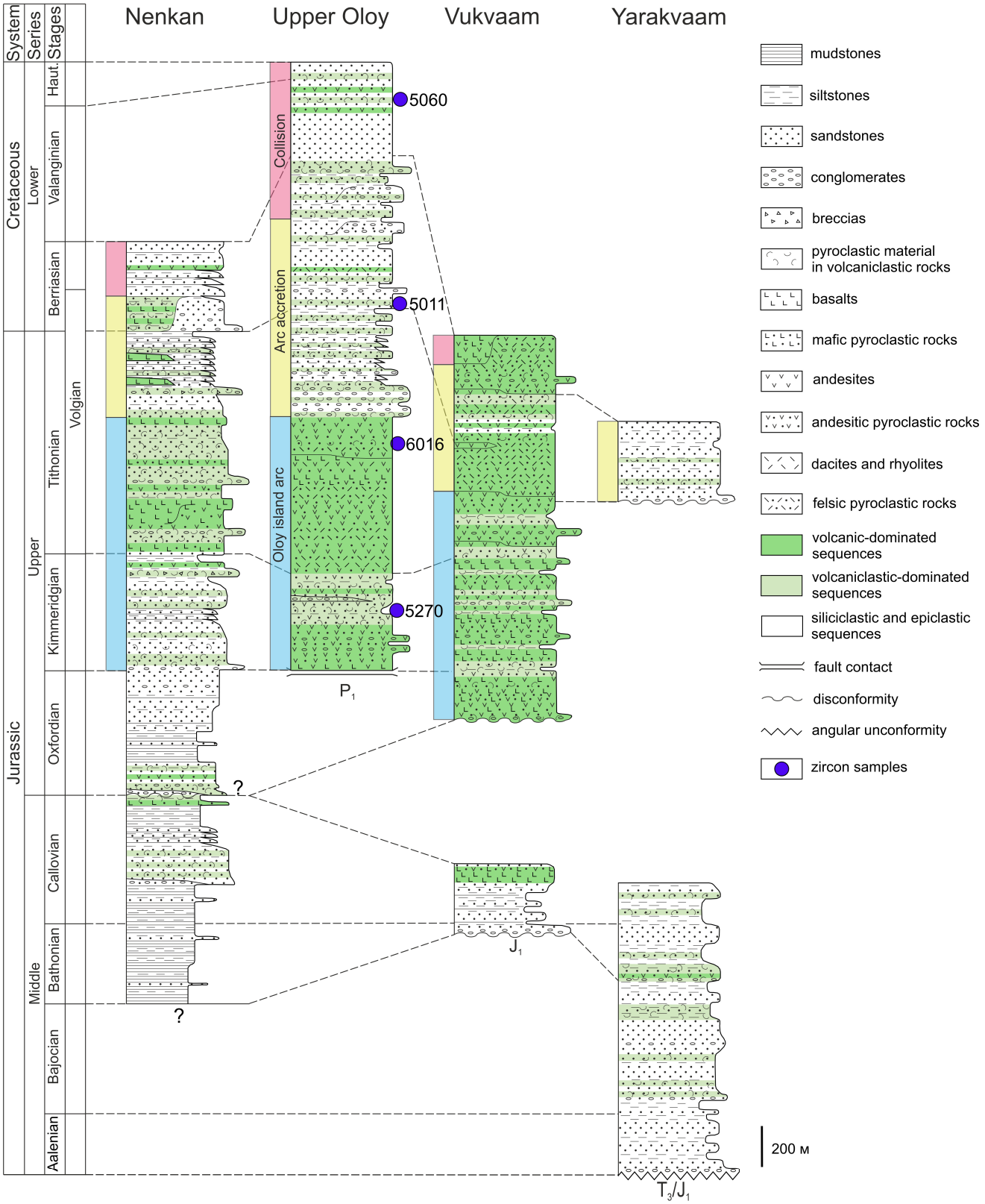


Figure 2. Correlation scheme of the Middle Jurassic–Lower Cretaceous volcanic–sedimentary deposits of the Kolyma–Omolon margin. Based on [15,31–33].

The Nenkan Zone has a continuous section from Bathonian to Berriasian. The underlying deposits have not been identified. The section begins with Bathonian black mudstones and siltstones containing rare, thin interbeds of sandstones. In addition to fine-grained siliciclastic rocks, the Callovian section comprises layers of volcaniclastic sandstones and a two-metre-thick layer of unsorted conglomerates (tilloids). Pebbles are represented by igneous rocks, such as andesites, basalts and diorite porphyrites, as well as sedimentary rocks, including siliceous mudstones and limestones. In adjacent areas, pebbly siltstones of the same level contain marbles, quartzites, quartz–mica schists and quartz. In the upper part of the Callovian section, crystal basaltic tuffs are present. The Upper Jurassic (Oxfordian?) section starts with volcaniclastic deposits and is followed by predominantly siliciclastic rocks. The presence of basal conglomerates in the lower part of the Upper Jurassic section is noted occasionally. An angular unconformity between the Middle and Upper Jurassic sequences has been established at one of the outcrops. It should be noted that the division of the Callovian–Oxfordian sequences is complicated due to the rare faunal remains. The Kimmeridgian–Berriasian sections show significant variability across different areas. In the central part of the zone, only the Lower–Middle Tithonian strata are composed of volcanic and volcaniclastic rocks. The Kimmeridgian and Upper Tithonian–Lower Berriasian sequences are mainly siliciclastic with intervals of volcaniclastic sandstones and, less commonly, andesitic tuffs. Along the western border of the zone, the Kimmeridgian and Upper Tithonian–Lower Berriasian deposits contain a greater number of volcaniclastic rocks and basalt or andesite–basalt flows. The Upper Berriasian strata are found in isolated areas, and they are siliciclastic with a large number of flora remains. A characteristic feature of the Nenkan Zone is the basaltic, less often andesite–basaltic, composition of volcanogenic rocks.

In the Upper Oloy Zone, a continuous section is established from the Kimmeridgian to the Lower Hauterivian. Upper Jurassic deposits have tectonic contact with Lower Permian mudstones and siltstones of the Berezov terrane. The Upper Jurassic–Lower Cretaceous section has a two-part structure. The Kimmeridgian–Middle Tithonian part is composed predominantly of volcanic rocks. They are overlain by Upper Tithonian volcaniclastic conglomerates and gravelstones. The pebbles mainly consist of volcanic rocks, and a large amount of pyroclastic material is present in the matrix. The Lower Cretaceous sequences are mainly composed of volcaniclastic and siliciclastic sandstones, conglomerates, siltstones and mudstones, with rare interbeds of tuffs.

The Vukvaam Zone stands out in the southwestern part of the Yarakvaam terrane. Bathonian basal conglomerates disconformably overlay Lower Jurassic siliciclastic and volcaniclastic deposits. Callovian sequences are predominantly composed of siliciclastic deposits. In the upper part of the Middle Jurassic section, a basalt flow 60–70 m thick is identified [32]. At the base of the Upper Jurassic section occur Oxfordian deposits, whose stratigraphic position remains ambiguous due to the scarcity of faunal finds. Upper Jurassic deposits disconformably overlay the Middle Jurassic section, occasionally with basal conglomerates. Common tuff welding indicates the onset of accumulation under continental conditions [32]. The Upper Jurassic–Lower Cretaceous (Oxfordian?–Berriasian) deposits have a predominantly volcanogenic composition (volcanic and volcaniclastic rocks). The lower part mainly consists of mafic to intermediate compositions with pillow basalt horizons, while the upper part predominantly consists of acid tuffs. Locally within the Upper Berriasian section, volcanic and volcaniclastic rocks of andesitic and basaltic composition occur [31,32]. This feature is specific to the Vukvaam Zone.

The Yarakvaam Zone has been identified in the northern part of the Yarakvaam terrane and has a distinct structure devoid of volcanic rocks. Middle Jurassic deposits (Aalenian–Callovian) lie with angular unconformity on predominantly siliciclastic Upper Triassic

and locally Lower Jurassic deposits. Siliciclastic deposits with interbeds of volcaniclastic sandstones and mudstones dominate the section. Rare horizons of andesitic tuffs are noted in the Bathonian part of the section [31,33]. The Middle Jurassic deposits are overlain by an Upper Tithonian–Lower Berriasian sequence with stratigraphic unconformity and basal conglomerates. This sequence is also predominantly siliciclastic, with local admixture of pyroclastic material.

2.3. Age and Composition of Upper Jurassic–Lower Cretaceous (Tithonian–Valanginian) Plutonic Rocks

Late Jurassic–Early Cretaceous plutons intrude the Tithonian–Berriasian volcanic–sedimentary deposits of the Oloy complex. The monzonitic Egdegkych Complex forms large massifs and the diorite-porphyritic Vesenninsky Complex forms small bodies adjacent to the Egdegkych massifs [11,18,20,21]. The U-Pb zircon ages of the Egdegkych Complex span the interval of 144–135 Ma [6,18,20,21,34]. Ages obtained for the granitoids of the Vesenninsky Complex range from 143 to 139 Ma [35]. Recently, in the southeast of the Baimka Trend, the Trekhglavy Complex, with ages ranging from 142 to 138 Ma, was identified. This complex consists of a series of moderately potassic gabbro to high-potassium leucogranite [19]. Within the Upper Oloy Zone, the Keyettyn Complex, comprising low-potassium rocks from gabbro to leucogranite, was established with dates ranging 147–140 Ma [15,19].

Late Jurassic plutons (147–145 Ma) within the Keyettyn Complex display suprasubduction geochemical signatures [19]. Granitoids of the Egdegkych, Vesenninsky and Trekhglavy complexes with moderate alkalinity include both high-potassium and adakite varieties. They are similar to high-silica adakites, slab-failure granitoids, and magmatic rocks of transform margins, whose formation was related to asthenosphere mantle upwelling in slab-failure settings [11]. These complexes formed over the course of the collision between the Kolyma–Omolon and Chukotka margins; they are post-subduction and syncollisional and not suprasubduction, as was previously thought [11]. The Baimka ore dextral strike-slip zone is also associated with this setting. Porphyry copper and epithermal gold–silver mineralization of the Baimka Trend is related to the Egdegkych and Vesenninsky complexes. The age of mineralization ranges from 137.9 to 142.7 Ma (Re-Os, molybdenite) and from 137 to 143 Ma (Rb-Sr, metasomatites) [17,34].

Within the Omolon terrane, the Namyndykan complex (144–138 Ma) is considered the analogue of the Egdegkych, Vesenninsky and Trekhglavy complexes [7]. It is represented by multiphase massifs ranging from gabbro to granite aplite. The major part of the plutons has a diorite–granodiorite composition.

3. Materials and Methods

The materials used in this work were compiled from regional-scale geological surveys conducted in 2019–2021 by specialists from the Karpinsky All-Russia Research Geological Institute in the Upper Oloy area (sheets Q-58-XXI, XXII). Detailed studies and numerous fauna and flora findings enabled correlation of fragmented outcrops and determination of the stratigraphic position of the Upper Jurassic–Lower Cretaceous formations in the Upper Oloy Zone [15]. Samples were collected from all units of the Kimmeridgian–Upper Hauterivian section (Figure 3).

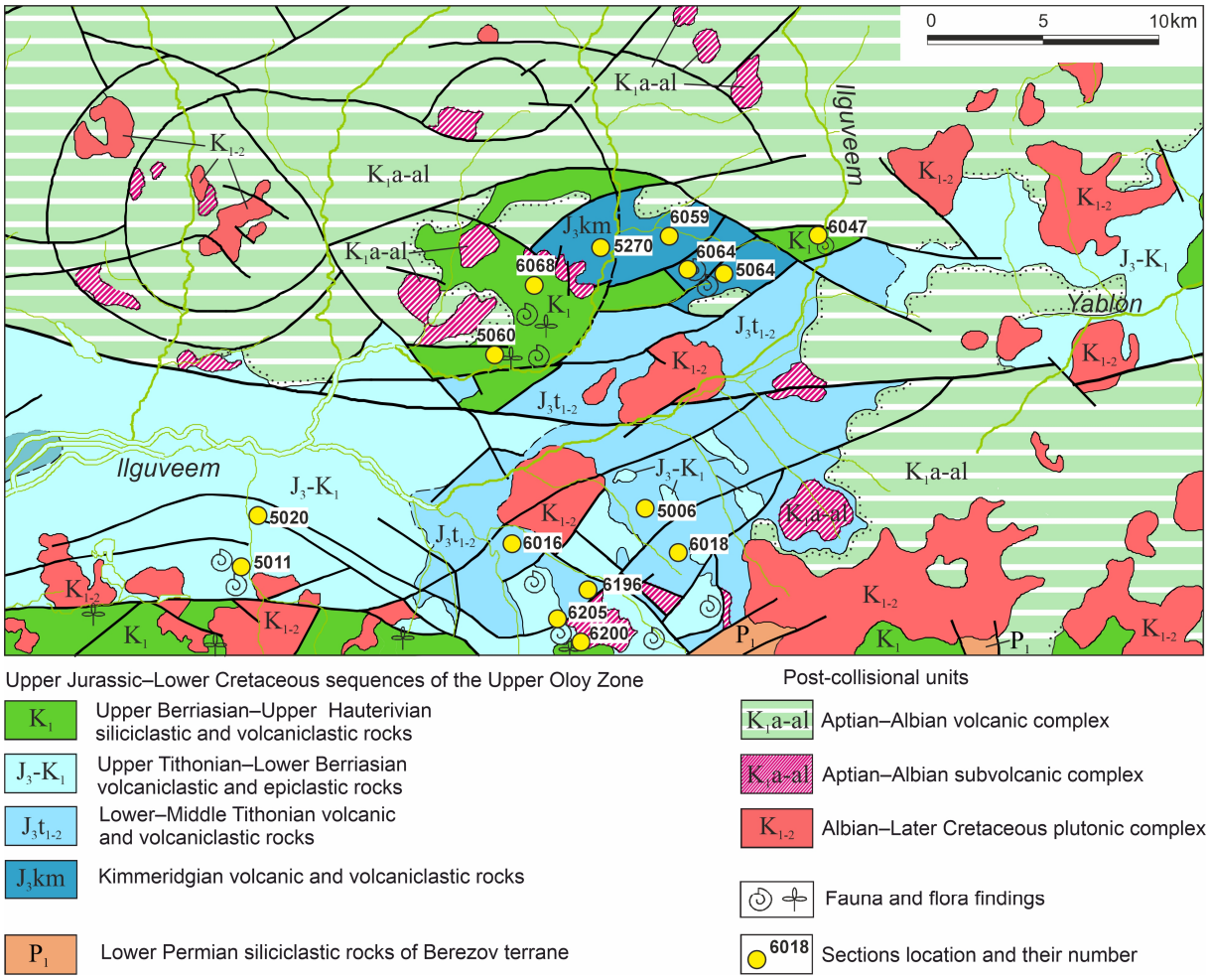


Figure 3. Geological map of the Upper Oloy area. Modified following [15].

Petrographic studies were performed on all volcaniclastic and siliciclastic rocks (41 samples) in the section. For the provenance study, sandstones with minimal content of synchronous volcanic material (16 samples) were selected from all the stratigraphic units identified during the geological survey. The Kimmeridgian deposits are represented by tuffites (sample 5064) and volcaniclastic sandstones (samples 5270, 6059 and 6064); the Lower and Middle Tithonian deposits by volcaniclastic sandstones (samples 6196 and 5006) and epiclastic sandstones (samples 6016 and 6018); the Upper Tithonian–Lower Berriasian deposits by epiclastic sandstones (samples 5011 and 6205) and epiclastic sandstones with sporadic gravel size fragments (samples 5011-2 and 5020); and the Upper Berriasian–Lower Hauterivian deposits by volcaniclastic sandstones (samples 6200 and 6068) and epiclastic sandstones (samples 5060 and 6047).

Rock-forming components of volcaniclastic deposits were classified into three groups based on their origin: (1) synchronous pyroclastic material, (2) resedimented volcanogenic material, and (3) siliciclastic (non-volcanic) material. According to Le Maitre nomenclature [36] the rocks were subdivided depending on the content of synchronous pyroclastic material into the following categories: more than 75%—tuff, from 25% to 75%—tuffite, less than 25%—use the prefix "volcaniclastic" (e.g., volcaniclastic sandstones). Siliciclastic rocks dominated by the redeposited volcanogenic fragments are termed epiclastic. Proportions were estimated in thin sections by visual petrographic analysis using templates.

Discrimination of sandstones was based on the counting components following the Gazzi–Dickinson methodology [37]. The calculation for each sample included more than

300 grains. To minimize the grain size effect, only grains sized from 0.1 to 0.25 mm were selected for the point-counting technique.

Petrographic studies were conducted using an optical polarizing microscope (Olympus BX-51, Olympus Corporation, Tokyo, Japan). Optical microscopy results were verified using a scanning electron microscope (Phenom XL G2, Thermo Fisher Scientific, Eindhoven, The Netherlands) equipped with an energy-dispersive spectrometer. Measurements were performed at an accelerating voltage of 15 kV, a beam current of 10–20 nA, and a measurement duration of 60 s.

To identify the alteration degree and source of the clastic material, geochemical studies (XRF and ICP-MS analyses) were conducted on nine samples of volcaniclastic and epiclastic sandstones.

The major element composition of sandstones was analyzed at the Chemical–Analytical Laboratory of the Geological Institute of the Russian Academy of Sciences by X-ray fluorescence using a sequential spectrometer (S8 Tiger, Bruker, Ettlingen, Germany) and Spectra-Plus software (v2017). The fundamental parameter method was used to take into account matrix effects in the Spectra-Plus software. A control sample of rock material rhyolite ORPT-1 (GeoPT37) from the International Association of Geoanalysts' Proficiency Testing programme for analytical geochemistry laboratories (IAG, GeoPT) was analyzed together with the studied samples.

The content of total iron (in the form of Fe_2O_3) was determined by XRF. The content of FeO was determined by wet chemistry (titration with potassium dichromate in sulfuric acid medium after acid decomposition of a sample in the absence of oxygen) in another portion of the same sample. To obtain the content of precisely Fe(III) (in the form of Fe_2O_3), the XRF data were corrected for the amount of iron (II) oxide obtained from the titration results.

The procedure for determining the carbon dioxide content of a rock sample involves dissolving calcium and magnesium carbonates (calcite, dolomite, and ankerite) in the rock in hydrochloric acid at low temperatures, absorbing the released carbon dioxide with a sodium hydroxide solution, precipitating the resulting carbonate ions with a barium chloride solution, and titrating the remaining free hydroxide ions with hydrochloric acid in the presence of phenolphthalein as an indicator. The carbon dioxide content is calculated by the difference between the amounts of hydrochloric acid used to titrate the sodium hydroxide solution before and after carbon dioxide absorption. Carbon dioxide is released by the hydrochloric acid and is absorbed by excess alkali in a hermetically sealed vessel.

The element composition was determined at the Analytical Certified Test Center of the Institute of Microelectronics Technology and High Purity Materials, Russian Academy of Sciences. Sandstones were decomposed in an autoclave (MKP-05 NPVF, ANKON-AT-2, Moscow, Russia). To control the complete dissolution of samples and possible losses during decompositions, each analyzed sample was doped with stable ^{161}Dy and ^{62}Ni isotopes. The contents of trace elements in obtained solutions were determined by inductively coupled plasma atomic emission mass spectrometry (ICAP-61, Thermo Jarrell Ash, Franklin, MA, USA) and inductively coupled plasma mass spectrometry (X-7, Thermo Elemental, Franklin, MA, USA). The following standards were used: alkaline agpaite granite SG-3 (GSO3333-85) and granodiorite, Silver Plume, Colorado, GSP-2 (United States Geological Survey).

Sm-Nd isotopic geochemical systematics were conducted on five samples. The Nd isotope composition was determined at the Center of Isotope Research of the Karpinsky All-Russian Geological Research Institute on a TRITON thermo-ionization mass spectrometer. Element concentrations were analyzed using the isotope dilution method with the addition of calibrated isotopic tracer. The measured value of the international standard JNdi-1 was $^{143}Nd/^{144}Nd = 0.512106 \pm 2$.

Detrital zircons from three of the most representative sandstone samples were dated using the LA-ICP-MS technique at the Geological Institute of the Russian Academy of Sciences. Analyses were carried out using an Element2 (Thermo Scientific, Bremen, Germany) sector-field ICP-MS coupled to an laser ablation system (NWR-213, Elemental Scientific, Omaha, NE, USA), employing a common protocol [38]. Data processing and visualization were performed using IsoplotR toolbox [39].

Separation of zircon grains was performed according to the standard procedure at the Geological Institute of the Russian Academy of Sciences. Samples (4–5 kg) were crushed to a grain size of approximately 0.25 mm. Water-table, magnetic, and heavy-liquid separation techniques were employed to concentrate zircon. Final handpicking of zircon grains was performed under binoculars. About 300 grains from each sample were randomly selected and mounted in epoxy resin discs. Optical and cathodoluminescence (CL) images were used for the selection of dating spots. These images were obtained with a scanning electron microscope (Vega 3, Tescan, Brno, Czech Republic). A total of 110 grains were analyzed per sample.

4. Results

4.1. Petrographic Composition

Volcaniclastic sandstones play a minor role in the Kimmeridgian section. The rocks show poor sorting and the material is either nonrounded or subangular. The matrix is glassy or contains an admixture of ash material (Figure 4A). The rock-forming components are dominated by fragments of intermediate and mafic volcanics (>80%, Figure 4C). Fragments of felsic volcanics and monomineralic components (quartz, feldspar and pyroxene) of volcanic origin are present in smaller quantities. The quartz content does not exceed 1% (rarely up to 5%) and generally occurs as small angular fragments. Feldspars (10%–20%) are represented by large, unrounded or subangular fragments with a volcanic habitus, often altered (Figure 4B). Polysynthetic twinning is found in individual grains ($An_{32–40}$ andesine). Pyroxenes appear as short prismatic crystalloclasts of clinopyroxene, close to euhedral forms, often fractured (Figure 4D).

Among the Lower–Middle Tithonian deposits, volcanic and pyroclastic rocks (tuffs) predominate. In the upper part of the section, volcaniclastic and epiclastic sandstones appear. Epiclastic sandstones are characterized by moderate sorting with grain roundness varying from poor to good. There is an admixture of synchronous pyroclastic material, but most of the volcaniclastic material is recycled. Lithoclasts predominate among the rock-forming components (44 to 81%). Monomineralic components include quartz (5%–21%), feldspar (13%–31%) and dark minerals (rarely up to 11%). Quartz is mainly present as angular monocrystals (Figure 5A,C), as well as polycrystalline varieties with sutured contours (Figure 5B), blocky structure or granulation occurring less frequently (Figure 5A). Feldspars are mostly plagioclase, represented by poorly rounded short-prismatic crystals, often with polysynthetic twinning ($An_{15–20}$, oligoclase) and larger, frequently strongly altered grains with embayments of volcanic origin (Figure 5C). Potassium feldspars account for approximately 10% of total feldspars, characterized by tartan twinning, myrmekites, and perthites (Figure 5B). Individual unrounded feldspars with oscillatory zoning are also present (Figure 5C). Clinopyroxenes clearly dominate among the dark minerals, while hornblende, biotite, and epidote are present in much smaller proportions. Rock fragments are predominantly composed of intermediate (Figure 5C) and felsic volcanic rocks, along with quartz–feldspar aggregates, where feldspars exhibit perthitic and myrmekitic intergrowths (Figure 5D). Single fragments of basalts and mudstones are also detected, with rarer occurrences of quartz–mica schists. Accessory minerals include zircon and titanite (Figure 5C), as well as apatite.

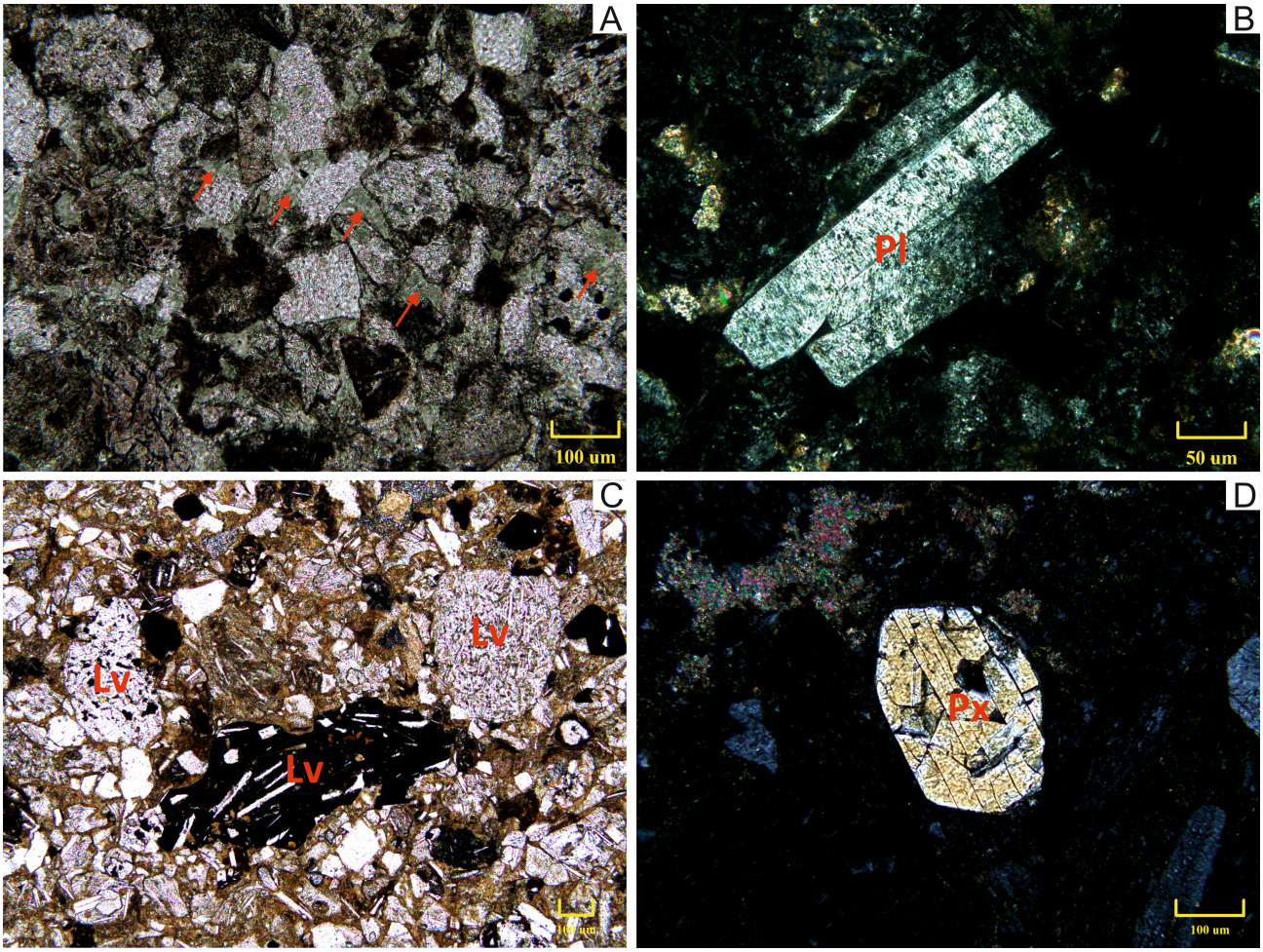


Figure 4. Photomicrographs of the Kimmeridgian volcaniclastic sandstone, sample 5270 (**A**,**B**), and tuffite, sample 5064 (**C**,**D**). Glassy matrix (**A**), crystalloclast of plagioclase (**B**), lithoclasts varying in shape and roundness (**C**), fractured crystalloclast of clinopyroxene, short prismatic close to euhedral form (**D**). Pl—plagioclase, Px—pyroxene, and Lv—fragments of volcanic rocks. Thin sections under plane-polarized light (**A**,**C**) and under cross-polarized light (**B**,**D**). The red arrows point to the glassy matrix.

The Upper Tithonian–Lower Hauterivian sequences are dominated by volcaniclastic and epiclastic rocks.

Upper Tithonian–Lower Berriasian sandstones are characterized by moderate to poor sorting and often contain gravel-sized grains (Figure 6A). The matrix is clayey with an admixture of ash material and occasionally glassy. Epiclastic sandstones display the following ratio of the main rock-forming components: quartz (5%–13%), feldspar (15%–28%), rock fragments (58%–80%) and dark minerals (rarely up to 10%). Quartz is represented by small (up to 0.2 mm), angular monocrystals (Figure 6B). Embayed grains or polycrystalline varieties are less common. Feldspars occur as small, euhedral, tabular crystals with polysynthetic twinning ($An_{28–35}$, oligoclase, and $An_{42–44}$, andesine), as well as larger grains (up to 0.4 mm) of volcanic appearance (Figure 6C). The potassium varieties are present as single highly altered grains with myrmekites and, rarely, perthites. Rock fragments are dominated by intermediate and felsic volcanics, with mafic ones being less common (Figure 6A). Notably, up to 30% of the total lithoclasts consist of volcaniclastic mudstones and siltstones, as well as quartz–mica schists. (Figure 6A,B). Both fine- and coarse-grained quartz–feldspar aggregates are also present. Among the dark minerals, in addition to pyroxenes and hornblende (Figure 6D), epidote can be found.

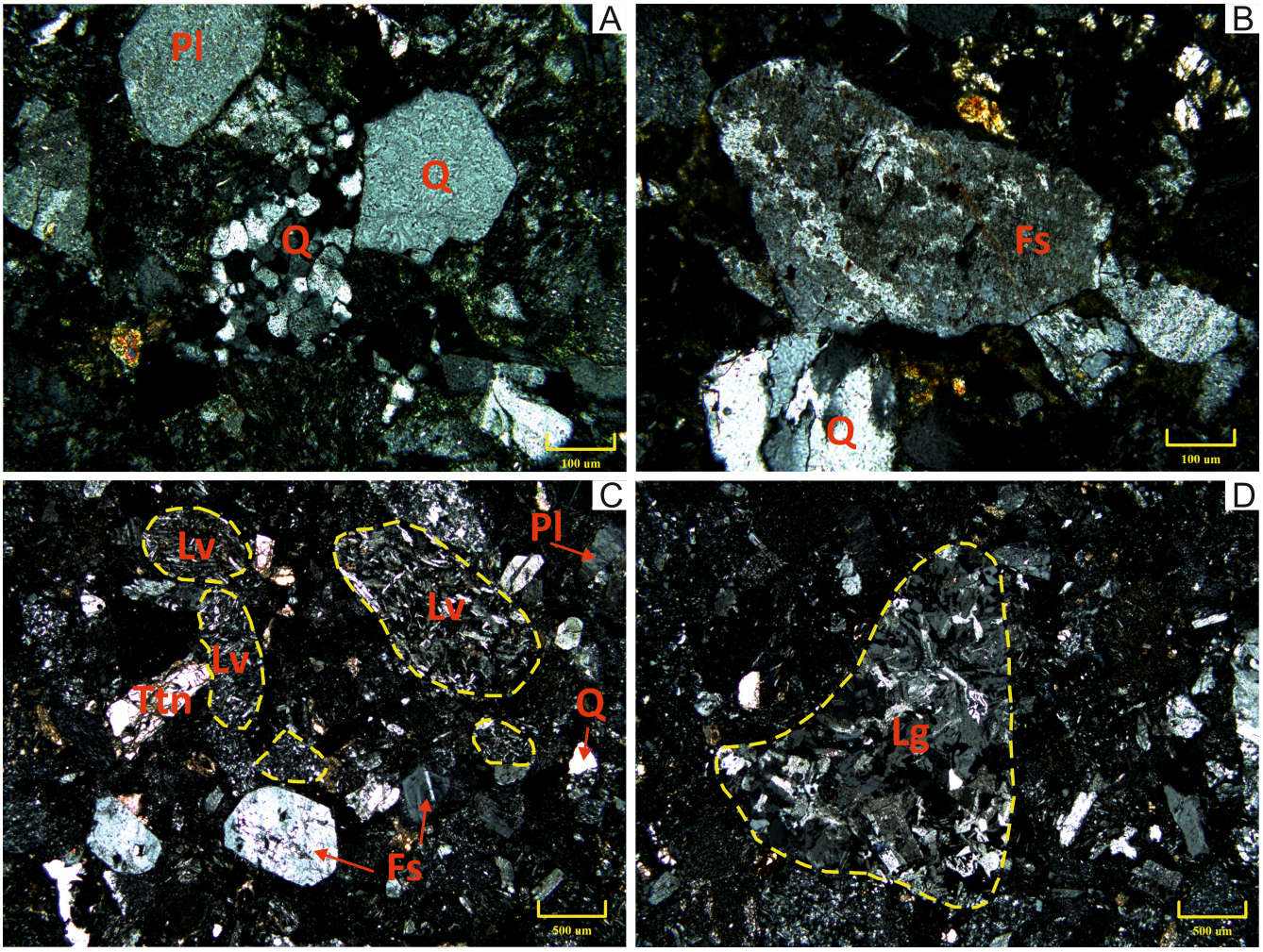


Figure 5. Photomicrographs of the Lower–Middle Tithonian epiclastic sandstones, sample 6016 (**A**,**B**) and sample 6018 (**C**,**D**). Monocrystal of quartz and polycrystalline quartz with granulation (**A**), fragment of polycrystalline quartz with sutured contours and feldspar grain with perthites (**B**), feldspars of volcanic origin (strongly altered grains with embayments and individual crystalloclast with oscillatory zoning), rounded andesitic lithoclasts (yellow dotted line) and a fairly large grain of titanite (**C**), gravel size grain of quartz–feldspar aggregate, with feldspars with myrmekitic intergrowths (**D**). Fs—K and K-Na feldspar, Q—quartz, Pl—plagioclase, Lv—fragments of volcanic rocks, Lg—fragments of granitic rocks, and Ttn—titanite. Thin sections under cross-polarized light (**A**–**D**).

Upper Berriasian–Lower Hauterivian epiclastic sandstones have a similar composition to the Upper Tithonian–Lower Berriasian varieties, differing in higher sorting grades (Figure 7A). Epiclastic sandstones are dominated by rock fragments (54%–68%) and feldspars (20%–25%). Quartz content varies from 6 to 20%. Volcaniclastic sandstones exhibit a high proportion of dark minerals (7%–13%). In addition to quartz monocrystals, Upper Berriasian–Lower Hauterivian sandstones contain polycrystalline varieties with sutured contours (Figure 7B), a blocky structure and granulation. Feldspars are predominantly plagioclases, represented by tabular-shaped fragments with lamellar twinning ($An_{27–30}$, oligoclase; rarely An_{45}, andesine). Larger grains are less common and often highly altered. Potassium feldspars do not exceed 15% of the total feldspar content and are also altered. They can be easily distinguished by the presence of perthites and myrmekites and, less commonly, by tartan twinning (Figure 7C). Among the lithoclasts, felsic (35%–55%), intermediate (30%–50%), and mafic (5%–10%) volcanic rocks dominate (Figure 7B–D). These fragments range from well-rounded to angular, with some lacking sharp outlines

and adopting conformable positions. The sandstones also contain variably altered quartz–feldspar aggregates and volcaniclastic mudstones. The main dark minerals are pyroxenes, while hornblende, epidote and biotite are less common.

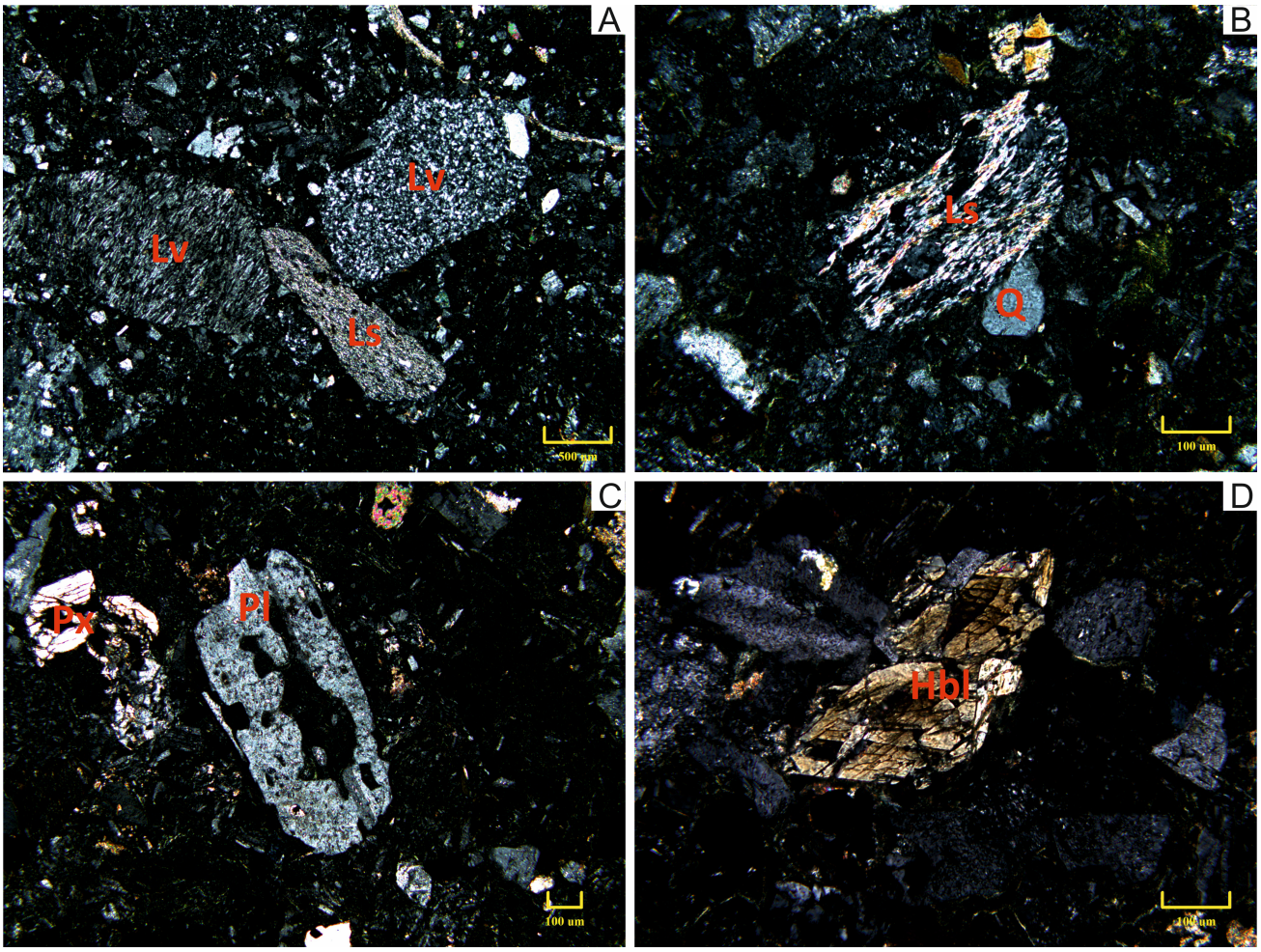


Figure 6. Photomicrographs of the Upper Tithonian–Lower Berriasian epiclastic sandstones with sporadic gravel size fragments, sample 5011-2 (**A**), and epiclastic sandstones, sample 5011 (**B**) and sample 5020 (**C**,**D**). Rock fragments (andesite, rhyolite and strongly altered siltstone) (**A**), grain of quartz–mica schist (**B**), large altered grain of feldspar with embayments and intensively fractured fragments of clinopyroxene (**C**), large crystalloclasts of hornblende (**D**). Q—quartz, Pl—plagioclase, Px—pyroxene, Hbl—hornblende, Lv—fragments of volcanic rocks, and Ls—fragments of sedimentary rocks and shales. Thin sections under cross-polarized light (**A**–**D**).

The ratio of the main rock-forming components of the studied sandstones in Dickinson's provenance diagram [37] shows the main contribution of the undissected and transitional-arc provenance for the Upper Jurassic–Lower Cretaceous deposits of the Upper Oloy Zone (Figure 8).

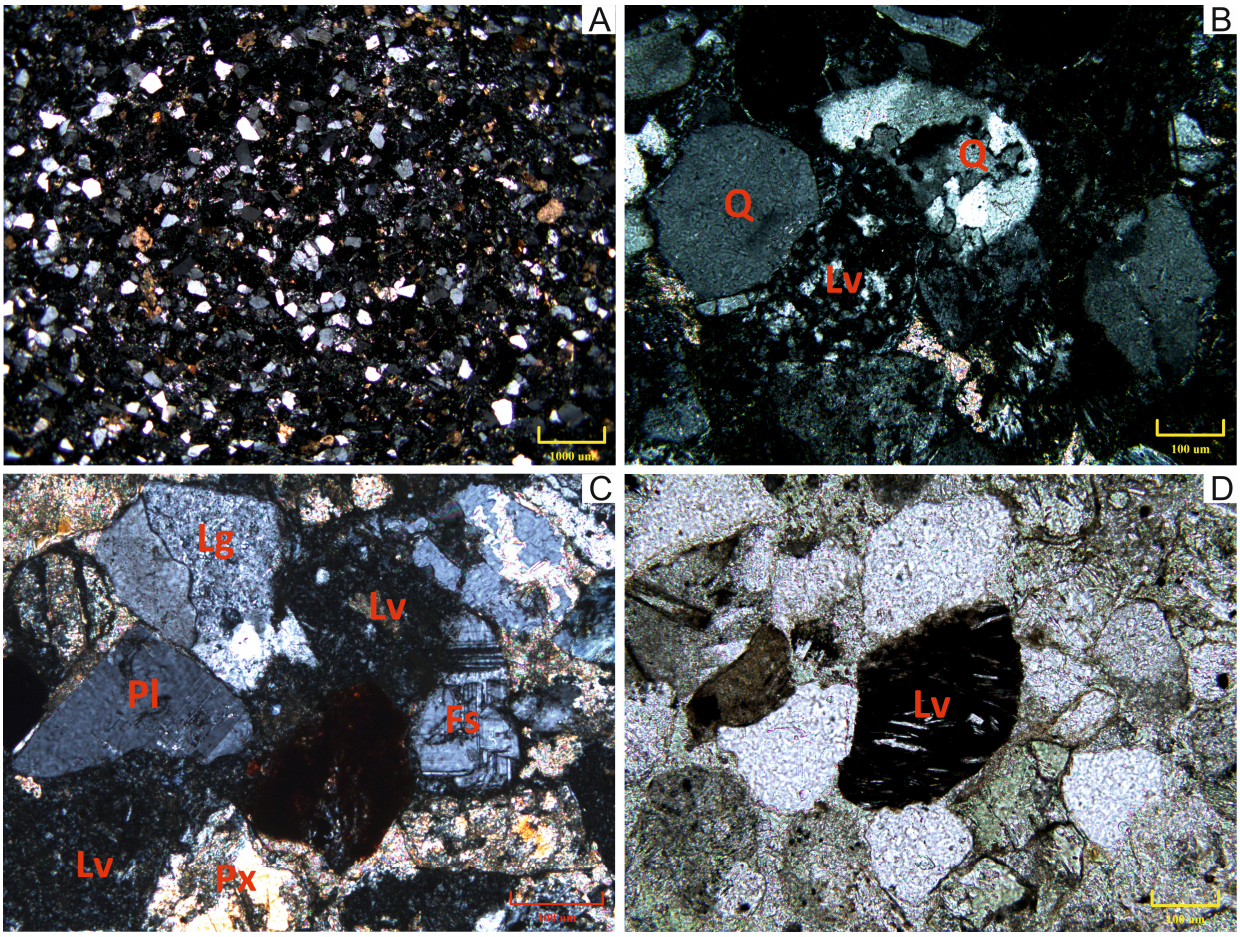


Figure 7. Photomicrographs of the Upper Berriasian–Lower Hauterivian epiclastic sandstones, sample 5060 (**A**,**B**), and volcaniclastic sandstones, sample 6068 (**C**,**D**). Well-sorted epiclastic sandstone (**A**), quartz grains (monocrystalline and polycrystalline varieties with sutured contours) and fragment of felsite (**B**), angular fragment of tabular-shaped plagioclase with lamellar, grain of potassium feldspar with tartan twinning, fragments of volcanic rocks and quartz–feldspar aggregate (**C**), and rounded grain of basalt (**D**). Fs—K and K-Na feldspar, Q—quartz, Pl—plagioclase, Px—pyroxene, Lv—fragments of volcanic rocks, and Lg—fragments of granitic rocks (quartz–feldspar aggregate). Thin sections under plane-polarized light (**D**) and under cross-polarized light (**A**–**C**).

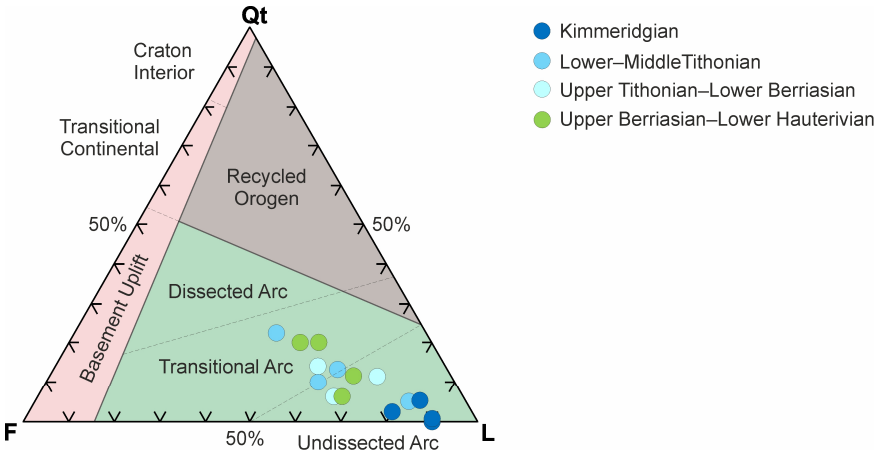


Figure 8. QtFL plot for the Upper Jurassic–Lower Cretaceous sandstones of the Upper Oloy Zone showing subdivisions according to inferred provenance type following [37]. Qt—total quartzose grains (monocrystalline quartz + polycrystalline quartz), F—feldspar grains, and L—unstable lithic fragments.

4.2. Major and Trace Element Geochemistry

Upper Jurassic–Lower Cretaceous sandstones of the Upper Oloy Zone are characterized by elevated iron and magnesium contents, moderately high titanium concentrations, and comparatively low silica contents, reflecting the prevalence of intermediate and mafic magmatic rocks in the source area. Low values of the Chemical Index of Alteration (CIA) ranging from 51.2 to 59.7 [40] indicate the predominance of fresh, recently exhumed rocks in their provenance. Low Zr/Sc ratios (3.2–7.4) combined with low Th/Sc in the sandstones' composition point to the absence of upward zircon accumulation in the section, as a result of maturation and recycling processes.

Petrographic investigations revealed that the deposits accumulated due to erosion from several sources. Therefore, the interpretation of the ratios of major and rare earth elements (REEs) in the sandstone composition is aimed at defining the tectonic setting of sedimentation. The graywacke composition of the sandstones permits the application of Bhatia diagrams [41]. These diagrams are highly informative as they distinguish various suprasubduction environments. The compositional data points of sandstones from the Upper Oloy Zone cluster within the field typical for deposits formed in an oceanic island-arc setting (Figure 9). They also demonstrate a temporal evolution in provenance composition, ranging from depleted to more differentiated features.

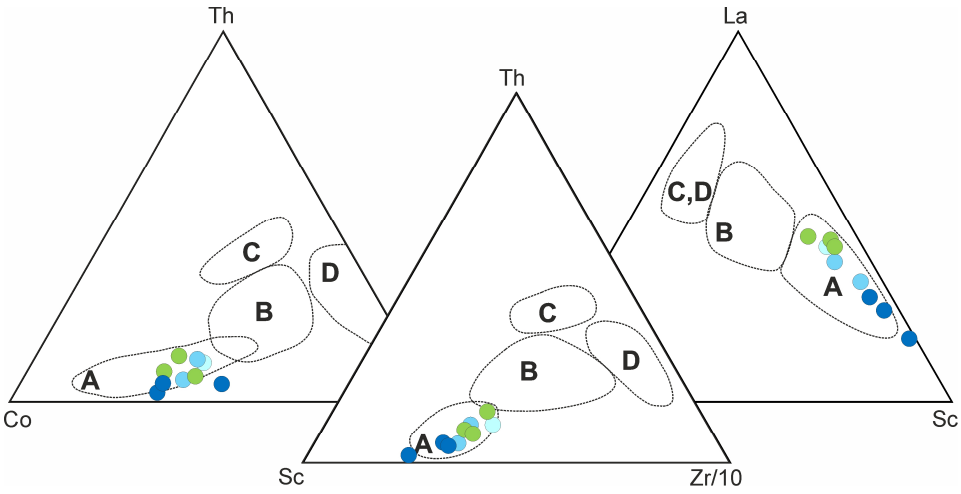


Figure 9. Tectonic setting discrimination plot after [41] for the Upper Jurassic–Lower Cretaceous sandstones of the Upper Oloy Zone. A—Oceanic island arc; B—Continental island arc; C—Active continental margins; D—Passive margins. Other symbols are explained in Figure 8.

Chondrite-normalized REE distribution spectra (Figure 10A) are similar across all studied samples. The rocks are strongly depleted in REEs, especially light REEs, compared to Post-Archean Australian Shale (PAAS). Total REE content varies from 63.4 to 107.1 ppm. The greatest differentiation between light and heavy REEs is observed in the youngest deposits. All deposits exhibit low Th/U ratios (1.6–2.7) with low concentrations of both Th and U, as well as extremely low Th/Sc ratios. Distribution is characterized by the absence of a europium minimum. A weakly positive europium anomaly is observed in some samples (Figure 10A).

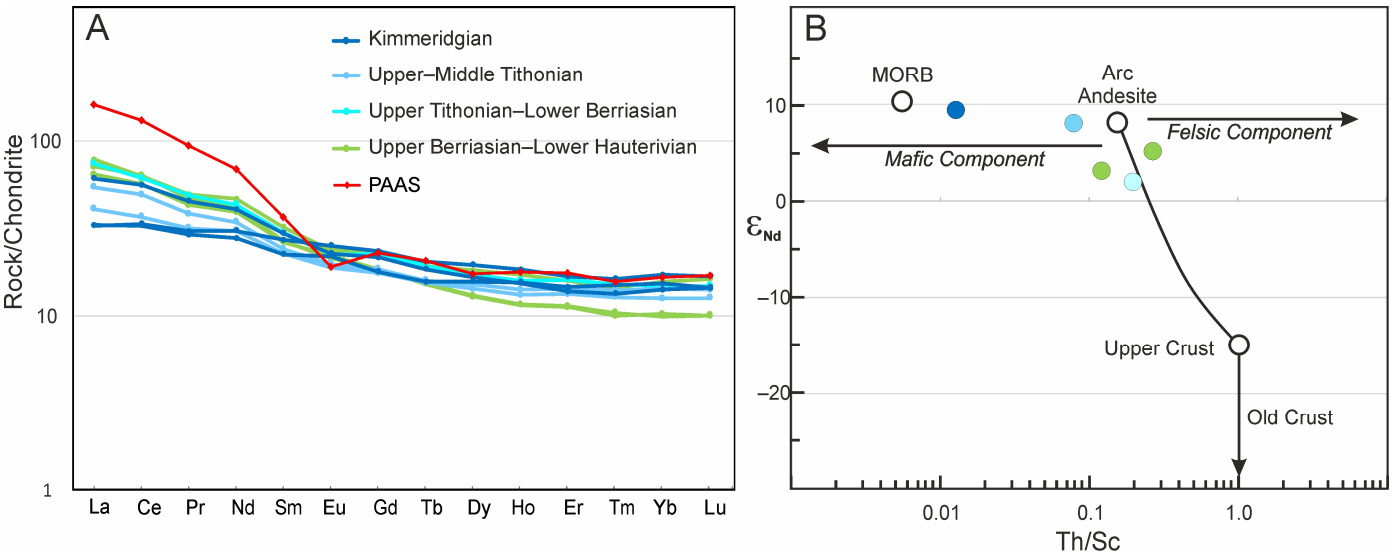


Figure 10. Chondrite-normalized REE distribution (**A**) and plot of εNd versus Th/Sc (**B**) for the Upper Jurassic–Lower Cretaceous sandstones of the Upper Oloy Zone. Chondrite values are from [42]. PAAS—Post-Archaean Average Shale from [43]. MORB—Mid-Ocean Ridge Basalt. Other symbols are explained in Figure 8.

4.3. Sm-Nd Isotopic Ratios

Sandstones of the Upper Oloy Zone exhibit positive epsilon neodymium (εNd) values ranging from +1.91 to +9.40, indicating a high proportion of juvenile material in their source area. The Kimmeridgian volcaniclastic sandstones show the highest εNd values. Based on the εNd and Th/Sc ratios, these sandstones approach the composition of MORB-type rocks (Figure 10B). The εNd parameter in younger deposits gradually increases. The position of the compositional data points of the sandstones on McLennan's discrimination diagram [44] indicates their accumulation in volcanic arc settings, with intermediate volcanic rocks predominating among the sources.

An increase in the epsilon parameter is accompanied by an increase in the Sm–Nd model ages of the sedimentary rocks. The T_{DM} values range from 177 Ma (Kimmeridgian sandstones) to 794 Ma (Valanginian sandstones). The Jurassic model age of the Kimmeridgian sandstones suggests the absence of an older basement in the provenance area.

4.4. U–Pb Detrital Zircon Dating

Zircons were not found in the Kimmeridgian volcaniclastic sandstones (sample 5270). Sample 6016 from the Lower–Middle Tithonian epiclastic sandstone contains several young grains corresponding to a sedimentation age of ~147.5 Ma, as well as a large Oxfordian–Toarcian population aged from 157 to 181 Ma, with a peak at 166 Ma, and a single grain of 188 Ma (Figure 11). Lower Berriasian epiclastic sandstone (sample 5011) yields a large Jurassic population and four grains in the 370–584 Ma time interval. The Jurassic age distribution includes a large population ranging from 141 to 155 Ma with two main peaks at 146 and 151 Ma, as well as seven isolated grains in the range of 159–193 Ma. The maximum depositional age (MDA), calculated from the five youngest grains, is 142.2 ± 0.9 Ma, corresponding to the Early Berriasian. The age distribution of detrital zircons from the Upper Valanginian epiclastic sandstone (sample 5060) reveals a dominant young population ranging from 129 to 154 Ma, with main peaks at 133.7, 141.7 and 149 Ma, as well as three Paleoproterozoic grains in the 1903–2013 Ma time interval.

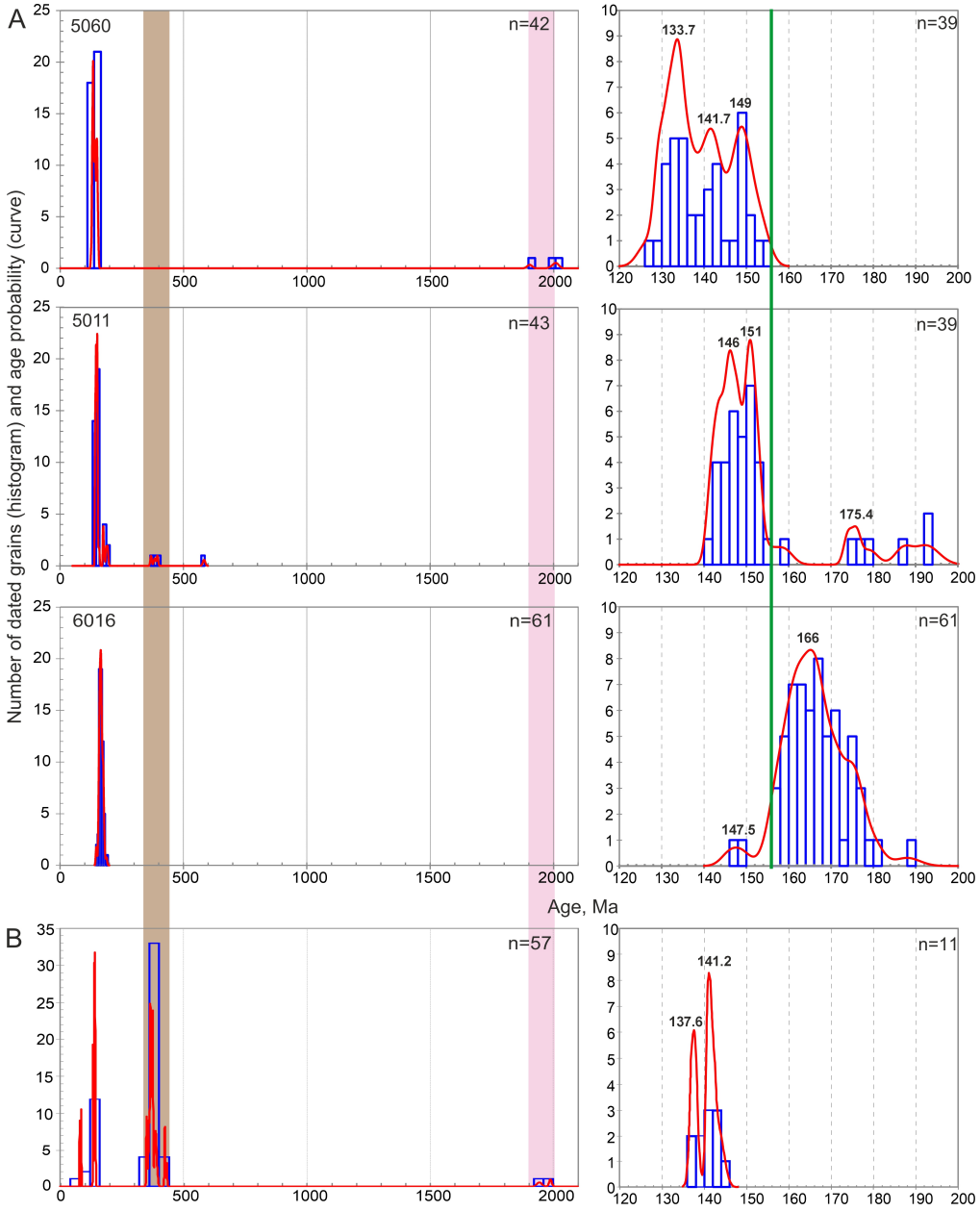


Figure 11. Distribution plots of detrital zircon ages from Upper Jurassic–Lower Cretaceous epiclastic sandstones in the ranges of 0–2100 Ma (on the **left**) and 0–200 Ma (on the **right**). The green line marks the Oxfordian–Kimmeridgian boundary, dividing two different stages of magmatic activity: the Middle Jurassic–Oxfordian and the Kimmeridgian–Valanginian (**A**). Stages of magmatic activity of the Omolon terrane based on zircon dating of volcanic and plutonic rocks; data from [7] (**B**).

5. Discussion

Middle Jurassic to Lower Cretaceous deposits of various zones of the Kolyma–Omolon margin overlie complexes of different ages. Within the Yarakvaam Zone, they lie with angular unconformity on Upper Triassic and locally Lower Jurassic strata of the Yarakvaam Paleozoic island-arc terrane. The disconformity with Lower Jurassic formations of the Yarakvaam terrane also occurs in the north of the Vukvaam Zone. The Upper Jurassic deposits of the Upper Oloy Zone are in tectonic contact with the Lower Permian strata of the Berezov Paleozoic island-arc terrane. Within the Nenkan Zone, the most continuous Middle Jurassic to Lower Cretaceous section is observed, with Bathonian mudstones and siltstones at its base. The underlying complexes have not been identified, suggesting the

absence of a pre-Jurassic basement in this part of the Kolyma–Omolon margin. These distinctive features support the interpretation of the Nenkan Zone and its framing as a Nenkan Jurassic oceanic island-arc terrane (Figure 1).

The correlation and comparison of Middle Jurassic–Lower Cretaceous volcanic–sedimentary sequences in the Yarakvaam, Vukvaam, Nenkan, and Upper Oloy zones allowed us to identify the main stage of volcanic activity associated with the formation of the Oloy arc (Figure 2). This stage is marked by volcaniclastic sequences with lavas of basalts, andesites, and more felsic varieties. Thus, only the Kimmeridgian to Lower Berriasian rocks can be attributed to the Oloy arc complex, as well as Oxfordian? strata in the Vukvaam Zone.

Detailed study of the Upper Jurassic–Lower Cretaceous volcanic–sedimentary sequences in the Upper Oloy Zone revealed a two-part architecture of the section (Figure 2). The Kimmeridgian–Middle Tithonian deposits are characterized by a predominance of volcanic and pyroclastic rocks. The Upper Tithonian–Lower Hauterivian part of the section consists of volcaniclastic and epiclastic rocks with conglomerates in the base. Sedimentary structures and faunal remains suggest accumulation in a shallow marine environment. The Cretaceous part of the sequence features the presence of plant detritus. A gradual transition from subaqueous to subaerial volcanism can also be observed.

The ratios of major rock-forming components in volcaniclastic and epiclastic sandstones indicate deposition in an undissected arc setting for Kimmeridgian deposits and an undissected to transitional arc setting for Tithonian–Lower Hauterivian successions (Figure 8). Detailed petrographic studies identified synchronous pyroclastic material at all levels of the section. The matrix exhibits signs of ash admixture and is frequently glassy (Figure 4A). The sandstones contain a large proportion of unstable components (Figure 4B,C, Figures 5C and 6C), particularly dark minerals (up to 13%). These minerals are typically nonrounded and characterized by increased fracturing (Figures 4D and 6D). Such crystalloclasts form when pyroclastic material enters water immediately, indicating proximity to active volcanism. Low CIA values and trends in Th/Sc and Zr/Sc ratios reflect an active tectonic regime with constant renewal in the source area. The ratios of major and trace elements in the geochemical composition of the sandstones indicate accumulation in an oceanic island-arc setting (see Figure 9). The isotopic-geochemical indicators of the sandstones ($\varepsilon Nd > +5$, $Eu/Eu^* \sim 1$, $Th/Sc < 1$, and $Th/U < 3$) also suggest a young undifferentiated arc provenance [44]. A small decrease in εNd and slight increase in Th/Sc are evident in Berriasian–Valanginian sandstones, indicating the erosion of more differentiated igneous rocks and input of clastic material from the continent.

Isotopic dating of detrital zircons from Tithonian, Upper Berriasian, and Upper Valanginian epiclastic sandstones also indicates a constant renewal of sources within the provenance area. The main sources are represented by complexes of the following ages: Late Jurassic–Early Cretaceous, Early–Middle Jurassic, Devonian, and Paleoproterozoic. Analysis of the distribution of young ages allows for the identification of two fertile (magmatic) stages at 130–154 Ma and 157–181 Ma with a Late Oxfordian–Early Kimmeridgian gap (Figure 11A). This may indicate the existence of two major subduction events in the region, separated by cessation of magmatic activity. Pre-Jurassic zircons are represented by single grains. Their ages correspond to the major stage of magmatism in the region and to the age of the Omolon crystalline basement (Figure 11B).

Thus, in the Kimmeridgian stage, the main sources were intra-oceanic volcanics lacking zircon grains. The rocks show a predominance of mafic to andesitic lithoclasts among the rock-forming components, with a minor amount of quartz. The isotopic-geochemical characteristics of the sandstones ($\varepsilon Nd > +9.39$, $Eu/Eu^* = 0.9–1.1$, and $Th/Sc < 0.01–0.07$) suggest the erosion of tholeiitic volcanic rock.

From the Tithonian time, older and differentiated volcanic–plutonic associations of intermediate to felsic composition were exposed in the provenance area. These supplied the main volume of material to the sedimentary basin during breaks between eruptions. The isotopic-geochemical characteristics of the epiclastic sandstones (εNd = +8.05, Eu/Eu* = 0.94–0.95, and Th/Sc = 0.08–0.18,), containing minor admixtures of synchronous pyroclastic material and single syn-sedimentary-age zircons, indicate an island-arc genesis and predominantly intermediate composition of this source. The Middle Jurassic–Oxfordian age of the magmatic association serving as the primary source is estimated based on detrital zircon dating.

During the Late Tithonian–Early Berriasian times, the residual basin was filled with sandy and coarse clastic material containing many volcanic pebbles. Volcanic activity in a distal source supplied pyroclastic material. Late Jurassic volcanic–plutonic associations of the Oloy complex began to dominate the hinterland with continued erosion of older, predominantly Early Jurassic associations. Additional sources of clastic material include older, siliciclastic and volcaniclastic rocks, variously altered and deformed, up to quartz–mica schists.

In the Late Berriasian–Early Hauterivian times, the erosion of the Late Jurassic–Early Cretaceous volcanic–plutonic associations continued. The presence of single ancient zircon grains in the rocks may be associated with the exposure and the onset of erosion of the old continental crust.

These changes in depositional environments and provenance in the Kimmeridgian–Lower Hauterivian volcano-sedimentary sequences of the Upper Oloy Zone indicate sedimentation during the transition from a subduction to collision regime. From the Kimmeridgian, the Oloy island arc existed near the Kolyma–Omolon margin, with one part situated on the oceanic plate (Nenkan terrane). A south-dipping subduction zone was directed towards the continent. Volcanic activity was recorded in all zones of the Oloy area except Yarakvaam (Figure 2). The oceanic island arc was also evident in the northern part of the South Anyui Ocean at this time [5,13].

Volcanic activity reached its widest extent in the Tithonian. Thick sequences of volcanic and pyroclastic rocks formed at this time in the Nenkan, Upper Oloy and Vukvaam zones. From the Middle Tithonian (~147 Ma), the Keyettyn Complex plutons were emplaced. These intrusive rocks are characterized by island-arc isotopic-geochemical signatures [15,19]. The beginning of the tectonic reorganization in the region is marked by the exhumation and erosion of Lower–Middle Jurassic island-arc complexes. Traces of this source were identified in the Yarakvaam Zone after the end of the Callovian stage [6]. Reorganization in this area occurred earlier, evidenced by the absence of sedimentation until the Late Tithonian (Figure 2).

From the Late Tithonian, the Oloy arc was accreted to the Kolyma–Omolon margin. Accretion was driven by the approach of the Chukotka microcontinent and general contraction of the South Anyui Basin. An accretionary prism formed along the Yarakvaam boundary. Clastic rocks within the prism contain fauna of Late Tithonian and Berriasian–Valanginian age [5]. The island-arc settings changed to an active continental margin with isolated remnant basins. A fore-arc basin formed within the Yarakvaam Zone. In the Upper Oloy Zone, erosion of Paleozoic complexes of the Kolyma–Omolon margin started to feed the residual basin (Figure 11). But the main source was the Late Jurassic volcanics of the exhumed Oloy arc. Alongside overall waning volcanism and uplifting of the territory, magmatic activity persisted in the Vukvaam Zone until the end of the Berriasian, producing predominantly pyroclastic rocks with volcanic horizons. The Vukvaam Zone is interpreted as a strike-slip zone formed over the course of the collision of the Kolyma–Omolon and Chukotka continents [11,17]. The Egdegkych, Vesenninsky, and Trekhglavy

plutonic complexes with high-potassium and adakite varieties were intruded during the Berriasian–Early Valanginian.

Depositional environments during the Valanginian–Early Hauterivian can be inferred only from epiclastic and volcaniclastic rocks with minor pyroclastic horizons in the Upper Oloy Zone. The main sources were previously formed Late Jurassic–Early Cretaceous rocks of the Oloy complex. The presence of single ancient zircon grains (~1.9–2.0 Ga) in the sandstones may be associated with the onset of erosion of the old crust in the basement of the Omolon craton (Figure 11).

During the Early Cretaceous Epoch, in the South Anyui Zone, predominantly siliciclastic and epiclastic deposits with a minor admixture of synchronous pyroclastic material accumulated. Despite the abundance of volcanic fragments in the sandstones, these contain a significant population of ancient (Proterozoic and Archean) zircon grains [6,31]. Some researchers [10,45] conclude that these sediments were deposited in a foreland basin during the Tithonian–Valanginian times. The main sources were Oloy complex and the ancient granitoids of the Omolon cratonic block. These conclusions suggest that the South Anyui Ocean closed prior to their accumulation [10,45]. Our results contradict this assumption. Signs of ancient crust erosion on the Kolyma–Omolon margin are not observed until the Valanginian stage. Moreover, pyroclastic rocks are finally recorded in the Upper Valanginian–Lower Hauterivian sequences, reflecting the closure of the South Anyui Ocean at this stage.

6. Conclusions

A comprehensive study of Kimmeridgian–Lower Hauterivian volcaniclastic and epiclastic rocks rich in fossils from the Upper Oloy Zone has revealed a change in sedimentation conditions and provenance in the back-arc basin of the Oloy arc. For the first time, U-Pb dating of detrital zircons from the Upper Jurassic–Lower Cretaceous sandstones of the Oloy complex was performed, allowing for the determination of the source rocks' age.

Integrating our results with previous studies permits the tracing of the evolution of magmatism and emphasizes several important stages in the development of the Kolyma–Omolon margin during the closure of the South Anyui Ocean:

- During the Kimmeridgian, the Oloy island arc existed on the southern margin of the South Anyui Ocean, with subduction directed towards the Kolyma–Omolon margin. Volcanics derived from a depleted mantle source and volcaniclastic rocks were formed by their disintegration and accumulation in the back-arc basin.
- In the Tithonian, the back-arc basin experienced reduction and compression due to the accretion of the arc onto the Kolyma–Omolon margin. The change in regime was caused by the approach of the Chukotka microcontinent and general contraction of the South Anyui Ocean. Plutonic complexes with suprasubduction characteristics are intruded. The Upper–Middle Jurassic island-arc series were exhumed into the erosion zone.
- From the Late Tithonian, the accretion of the Oloy arc to the Kolyma–Omolon margin caused continental rise and a gradual waning of volcanism. Sedimentation continued in the residual back-arc and fore-arc basins. The provenance area comprises Late Jurassic volcanic–plutonic series of the Oloy arc and Palaeozoic altered and deformed rocks.
- In the Berriasian, the slab failure initiated the emplacement of numerous magmatic rocks with various compositions across the Kolyma–Omolon margin (Egdegkych, Vesenninsky, Trekhglavy and Namyndykan complexes). Magmatic activity in the strike-slip zone on the border with the Yarkvaam Paleozoic paleo-arc fragment continued until the Middle Valanginian. Large porphyry–epithermal ore-magmatic systems formed here.

- The Valanginian period was characterized by an active phase of collision, which led to general uplift, a reduction in marine sedimentation, and cessation of volcanism by the Early Hauterivian time.

Supplementary Materials: The following supporting information can be downloaded at: https://www.mdpi.com/article/10.3390/min16040407/s1, Table S1: Petrographic composition; Table S2: Major element geochemistry; Table S3: Trace element geochemistry; Table S4: Sm–Nd isotopic ratios; Table S5: U–Pb dating of detrital zircons.

Author Contributions: Conceptualization and methodology, E.V.; validation, E.V., A.K. and E.S.; formal analysis, E.V.; field work and sampling, E.S. and A.G.; data curation, E.V. and E.S.; writing—original draft preparation, E.V.; writing—review and editing, A.K. and E.S.; visualization, E.V. and E.S.; supervision, A.K.; project administration and funding acquisition, E.V. All authors have read and agreed to the published version of the manuscript.

Funding: This research was supported by the Russian Science Foundation, Project No. 24-27-00352.

Data Availability Statement: Data are available as the Supplementary Materials that are referred to in this contribution.

Acknowledgments: The authors thank S.D. Sokolov and E.P. Isaeva for helpful consultations, critical discussions and support during the preparation of this manuscript. We are very grateful for detailed and constructive comments by Georgia Pe-Piper and three anonymous reviewers that helped to improve the original version of the manuscript.

Conflicts of Interest: The authors declare no conflicts of interest.

References

1. Natal'in, B.A. *Early Mesozoic Eugeosyncline Systems of the Northern Part of the Pacific Rim*; Nauka: Moscow, Russia, 1984; 136p.
2. Parfenov, L.M.; Natapov, L.M.; Sokolov, S.D.; Tsukanov, N.V. Terrane analysis and accretion in northeast Asia. *Isl. Arc* **1993**, *2*, 35–54. [CrossRef]
3. Nokleberg, W.J.; Parfenov, L.M.; Monger, J.W.H.; Norton, I.O.; Khanchuk, A.I.; Stone, D.B.; Scotese, C.R.; Scholl, D.W.; Kazuya, F. *Phanerozoic Tectonic Evolution of the Circum-North Pacific*; U.S. Geological Survey Professional Paper; U.S. Geological Survey: Reston, VA, USA, 2000; 122p. [CrossRef]
4. Khanchuk, A.I.; Rodionov, S.M.; Goryachev, N.A.; Popov, V.K.; Golozubov, V.V.; Naumova, V.V. Geodynamics, Magmatism and Metallogeny of the Russian East. In *2 Books*; Khanchuk, A.I., Mun, N.S., Eds.; Dalnauka: Vladivostok, Russia, 2006; 526p.
5. Sokolov, S.D.; Tuchkova, M.I.; Ledneva, G.V.; Luchitskaya, M.V.; Ganelin, A.V.; Vatrushkina, E.V.; Moiseev, A.V. Tectonic position of the South Anyui Suture. *Geotectonics* **2021**, *55*, 697–716. [CrossRef]
6. Amato, J.M.; Toro, J.; Akinin, V.V.; Hampton, B.A.; Salnikov, A.S.; Tuchkova, M.I. Tectonic evolution of the Mesozoic South Anyui suture zone, eastern Russia: A critical component of paleogeographic reconstructions of the Arctic region. *Geosphere* **2015**, *11*, 1530–1564. [CrossRef]
7. Akinin, V.V.; Miller, E.L.; Toro, J.; Prokopiev, A.V.; Gottlieb, E.S.; Pearce, S.; Polzunenkov, G.O.; Trunilina, V.A. Episodicity and the dance of late Mesozoic magmatism and deformation along the northern circum-Pacific margin: North-eastern Russia to the Cordillera. *Earth-Sci. Rev.* **2020**, *208*, 103272. [CrossRef]
8. Luchitskaya, M.V.; Sokolov, S.D. Stages of Granitoid Magmatism and Formation of the Continental Crust of Eastern Arctic. *Geotectonics* **2021**, *55*, 717–739. [CrossRef]
9. Tikhomirov, P.L.; Luchitskaya, M.V.; Prokofiev, V.Y.; Akinin, V.V.; Miller, E.L.; Isaeva, E.P.; Palechek, T.N.; Starikova, E.V.; Boldyreva, A.I.; Wiegand, B. Evolution of Aptian and Albian Magmatism of Western and Northern Chukotka (Northeast Russia) Based on Zircon U-Pb Geochronology and Rock Geochemistry. *Int. Geol. Rev.* **2024**, *66*, 607–632. [CrossRef]
10. Miller, E.; Soloviev, A.; Kuzmichev, A.; Gehrels, G.; Toro, J.; Tuchkova, M. Jurassic and Cretaceous foreland basin deposits of the Russian Arctic: Separated by birth of the Makarov Basin? *Nor. J. Geol.* **2008**, *88*, 201–226.
11. Khanchuk, A.I.; Luchitskaya, M.V.; Vatrushkina, E.V.; Katkov, S.M.; Canhimbue, L.S. Early Cretaceous Adakite and High-Potassium Granitoids as Indicators of the Post-Subduction Environment for the Formation of Porphyry Copper Deposits in the Baim Ore Zone of Chukotka. *Russ. J. Pac. Geol.* **2025**, *19*, 555–572. [CrossRef]
12. Vatrushkina, E.V.; Tuchkova, M.I.; Sokolov, S.D. Suprasubduction Volcanism of Chukotka Terrane in the Late Jurassic–Early Cretaceous (Arctic Region, Russia). *Geotectonics* **2019**, *53*, 713–725. [CrossRef]

13. Moiseev, A.V.; Maskaev, M.V.; Ulyanov, D.K.; Sokolov, S.D.; Belyatsky, B.V. Kulpolnei Volcanic Complex of the South Anyui Suture (West Chukotka): Composition, Age, and Paleotectonic interpretations. *Dokl. Earth Sci.* **2021**, *499*, 564–569. [CrossRef]
14. Lychagin, P.P.; Dylevsky, E.F.; Shpikerman, V.I.; Likman, V.B. *Magmatism of the Central Regions of the North-East of the USSR*; Far Eastern Branch of the USSR Academy of Sciences: Vladivostok, Russia, 1989; 120p.
15. Starikova, E.V.; Gagieva, A.M.; Konovalov, A.L.; Vatrushkina, E.V.; Akinin, V.V. Upper Jurassic–Lower Cretaceous deposits of the eastern part of the Oloy Zone: Stratigraphy, geochemistry, age, and geodynamic setting. *Russ. J. Pac. Geol.* **2023**, *17*, 297–321. [CrossRef]
16. Shephard, G.E.; Müller, R.D.; Seton, M. The tectonic evolution of the Arctic since Pangea breakup: Integrating constraints from surface geology and geophysics with mantle structure. *Earth-Sci. Rev.* **2013**, *124*, 148–183. [CrossRef]
17. Chitalin, A.F.; Baksheev, I.A.; Nikolaev, Y.N. Porphyry Copper and Epithermal Gold–Silver Mineralization of the Baimka Ore Zone, Western Chukotka, Russia. *Geol. Ore Depos.* **2024**, *66*, 21–41. [CrossRef]
18. Kara, T.V. New data on the age of igneous complexes of the Alazey–Oloy Foldbelt (Western Chukotka). *Russ. J. Pac. Geol.* **2018**, *12*, 549–557. [CrossRef]
19. Konovalov, A.L.; Cherkashin, A.V.; Starikova, E.V.; Surin, T.N.; Gagieva, A.M. Early Cretaceous granitoid complexes of the Oloy zone (Western Chukotka). *Bull. North-East Sci. Cent.* **2024**, *2*, 3–25. [CrossRef]
20. Kara, T.V.; Tikhomirov, P.L.; Demin, A.D. New data on the age of magmatic events in oloy tectonic zone, West Chukotka area (evidences from zircon U–Pb dating). *Dokl. Earth Sci.* **2019**, *489*, 1277–1280. [CrossRef]
21. Chitalin, A.F.; Baksheev, I.A.; Nikolaev, Y.N.; Djedjeya, G.T.; Khabibullina, Y.N.; Müller, D. Porphyry Cu–Au ± Mo mineralization hosted by potassic igneous rocks: Implications from the giant Peschanka porphyry deposit, Baimka Trend (North East Siberia, Russia). *Geol. Soc. Lond. Spec. Publ.* **2022**, *513*, 323–349. [CrossRef]
22. Sokolov, S.D.; Lobkovsky, L.I.; Vernikovsky, V.A.; Tuchkova, M.I.; Sorokhtin, N.O.; Kononov, M.V. Late Mesozoic-Cenozoic tectonics and geodynamics of the east Arctic Region. *Russ. Geol. Geophys.* **2022**, *64*, 324–341. [CrossRef]
23. Tuchkova, M.I.; Sokolov, S.D.; Isakova, T.N.; Filimonova, T.V.; Petrov, O.L.; Vatrushkina, E.V.; Moiseev, A.V.; Kossovaya, O.L.; Verzhbitsky, V.E. Carboniferous carbonate rocks of the Chukotka fold belt: Tectonostratigraphy, depositional environments and paleogeography. *J. Geodyn.* **2018**, *120*, 77–107. [CrossRef]
24. Tuchkova, M.I.; Sokolov, S.; Kravchenko-Berezhnoy, I.R. Provenance analysis and tectonic setting of the Triassic clastic deposits in western Chukotka, northeast Russia. *Stephan Mueller Spec. Publ. Ser.* **2009**, *4*, 177–200. [CrossRef]
25. Tikhomirov, P.L.; Kalinina, E.A.; Kobayashi, K.; Nakamura, E. Late Mesozoic silicic magmatism of the North Chukotka area (NE Russia): Age, magma sources, and geodynamic implications. *Lithos* **2008**, *105*, 329–346. [CrossRef]
26. Akinin, V.V.; Zhulanova, I.L. Age and geochemistry of zircon from the oldest metamorphic rocks of the Omolon Massif (Northeast Russia). *Geochem. Int.* **2016**, *54*, 651–659. [CrossRef]
27. Zonenshain, L.P.; Kuzmin, M.I.; Natapov, L.M. *Geology of the USSR: A Plate-Tectonic Synthesis*; Page, B.M., Ed.; American Geophysical Union: Washington, DC, USA, 1990; 242p.
28. Akinin, V.V.; Polzunenkov, G.O.; Prokopiev, A.V.; Brusnitsyna, E.A. Magmatism of the Omolon Cratonal Terrane (Northeastern Russia): Geochronology, Geochemistry, and Geodynamics. *Russ. Geol. Geophys.* **2025**, *66*, 379–402. [CrossRef]
29. Lychagin, P.P.; Dylevsky, E.F.; Likman, V.B. Magmatism of the Omolon Middle Massif. News of the USSR Academy of Sciences. *Geol. Ser.* **1990**, *7*, 17–29.
30. Ganelin, A.V. *Ophiolite Complexes of Western Chukotka (Structure, Age, Composition, Geodynamic Settings of Formation)*; Sokolov, S.D., Ed.; GEOS: Moscow, Russia, 2017; 178p.
31. Isaeva, E.P.; Zvizda, T.V.; Lazareva, E.I.; Mazurkevich, K.N.; Paderin, P.G. *State Geological Map of the Russian Federation. Scale 1:1000,000. Third Generation; Chukotka Series; Sheet Q-58–Aliskerovo. Explanatory Note*; Markovskyi, B.A., Ed.; VSEGEI: Saint Petersburg, Russia, 2019; 371p.
32. Parakecov, K.V.; Parakecova, G.I. *Stratigraphy and Fauna of the Upper Jurassic and Lower Cretaceous Deposits of the North-East of the USSR*; Nedra: Moscow, Russia, 1989; 210p.
33. Shekhovtsov, V.A.; Glotov, S.P. *The State Geological Map of the Russian Federation, Scale 1:200,000; Oloy Series; Sheet Q-58-XI, XII. Explanatory Note*; Sokolov, S.D., Ed.; Ministry of Natural Resources Russian Federation: Moscow, Russia; VSEGEI: Saint Petersburg, Russia, 2001; 106p.
34. Kotova, M.S.; Nagornaya, E.V.; Anosova, M.S.; Kostitsyn, Y.A.; Baksheev, I.A.; Nikolaev, Y.N.; Kalko, I.A. Dating of metasomatic process and ore-bearing granitoids of copper porphyry deposits of the Nakhodka ore field (Western Chukotka). In *Geochronological Isotope Systems, Methods of Their Study, Chronology of Geologic Processes: Proceedings of the Russian Conference on Isotope Geochronology*; IGEM RAN: Moscow, Russia, 2012; pp. 181–184.
35. Chitalin, A.F.; Baksheev, I.A.; Nikolaev, Y.N.; Nagornaya, E.; Khabibulina, Y.; Nikolaeva, I.; Kalko, I.; Muller, D. Porphyry-epithermal Cu-Mo-Au–Ag mineralization in the Nakhodka ore field, Baimka Trend, Chukotka, Russia: A geological, mineralogical, and geochemical perspective. *Miner. Depos.* **2023**, *58*, 287–306. [CrossRef]

36. Le Maitre, R.W.; Streckeisen, A.; Zanettin, B.; Le Bas, M.J.; Bonin, B.; Bateman, P. *Igneous Rocks: A Classification and Glossary of Terms*, 2nd ed.; Cambridge University Press: Cambridge, UK, 2002; 252p. [CrossRef]
37. Dickinson, W.R. Interpreting provenance relations from detrital modes of sandstones. In *Provenance of Arenites*; Zuffa, G.G., Ed.; Springer: Dordrecht, The Netherlands, 1985; pp. 333–361. [CrossRef]
38. Sheshukov, V.S.; Kuzmichev, A.B.; Dubenskiy, A.S.; Okina, O.I.; Degtyarev, K.E.; Kanygina, N.A.; Kuznetsov, N.B.; Romanjuk, T.V.; Lyapunov, S.M. U–Pb zircon dating by LASF-ICPMS at Geological Institute GIN RAS (Moscow). In Proceedings of the 10th International Conference of the Analysis of Geological and Environmental Materials, Sydney, NSW, Australia, 8–13 July 2018; 63p.
39. Vermeesch, P. IsoplotR: A free and open toolbox for geochronology. *Geosci. Front.* **2018**, *9*, 1479–1493. [CrossRef]
40. Nesbitt, H.W.; Young, G.M. Early Proterozoic climates and plate motions inferred from major element chemistry of lutites. *Nature* **1982**, *299*, 715–717. [CrossRef]
41. Bhatia, M.R.; Crook, K.A.W. Trace element characteristics of graywackes and tectonic setting discrimination of sedimentary basins. *Contr. Mineral. Pet.* **1986**, *92*, 181–193. [CrossRef]
42. Sun, S.S.; McDonough, W.F. Chemical and isotopic systematics of oceanic basalts: Implication for mantle composition and processes. *Geol. Soc. Spec. Publ.* **1989**, *42*, 313–345. [CrossRef]
43. Nance, W.B.; Taylor, S.R. Rare earth element patterns and crustal evolution–I. Australian post–Archean sedimentary rocks. *Geochim. Cosmochim. Acta* **1976**, *40*, 1539–1551. [CrossRef]
44. McLennan, S.M.; Hemming, S.; McDaniel, D.K.; Hanson, G.N. Geochemical approaches to sedimentation, provenance and tectonics. In *Processes Controlling the Composition of Clastic Sediments*; Johnsson, M.J., Basu, A., Eds.; Geological Society of America: McLean, VA, USA, 1993; Volume 285, pp. 21–40. [CrossRef]
45. Miller, E.L.; Meisling, K.E.; Akinin, V.V.; Brumley, K.; Coakley, B.J.; Gottlieb, E.S.; Hoiland, C.W.; O'Brien, T.M.; Soboleva, A.; Toro, J. Circum-Arctic Lithosphere Evolution (CALE) Transect C: Displacement of the Arctic Alaska–Chukotka microplate towards the Pacific during opening of the Amerasia Basin of the Arctic. *Geol. Soc. Lond. Spec. Publ.* **2018**, *460*, 57–120. [CrossRef]

Disclaimer/Publisher's Note: The statements, opinions and data contained in all publications are solely those of the individual author(s) and contributor(s) and not of MDPI and/or the editor(s). MDPI and/or the editor(s) disclaim responsibility for any injury to people or property resulting from any ideas, methods, instructions or products referred to in the content.